Self-Assembly of Flowerlike AlOOH (Boehmite) 3D Nanoarchitectures

Jun Zhang, Sujing Liu, Jing Lin, Haisheng Song, Junjie Luo, E. M. Elssfah, E. Ammar, Yang Huang, Xiaoxia Ding, Jianming Gao, Shouren Qi, and Chengcun Tang*

Department of Physics, Central China Normal University, Wuhan 430079, P.R. China

Received: April 4, 2006; In Final Form: June 1, 2006

In this work, a hydrothermal route using an ethanol−water solution to progressively synthesize a sequence of flowerlike three-dimensional γ-AlOOH boehmite nanostructures without employing templates or matrixes for self-assembly is presented. The flowerlike boehmite nanoarchitectures exhibit three hierarchies of self-organization, i.e., single-crystalline nanorods, nanostrips, and bundles, which are characterized by scanning and transmission electron microscopy. The sequence of products obtained after different processing times indicates a self-assembly mechanism. The hydrogen bonding on the surface of nanorods or nanostrips possibly plays a key role, as identified by FTIR spectra of the products after they had been heated to 1000 °C. The specific surface area and pore-size distribution of the obtained product as determined by gas-sorption measurements show that the boehmite nanoarchitectures exhibit high BET surface area and porosity properties.

Introduction

Current challenges in the synthesis of nanomaterials essentially include morphological control and the assembly of ensembles of nanomaterials. For single nanostructured building blocks, control of the size, shape, and crystalline structure is of importance. Self-assembly of nanostructured building blocks has attracted significant interest in materials synthesis and device fabrication. A basic growth mechanism involving particle-oriented aggregation was conceptually termed "oriented attachment" by Penn and Banfield et al.[1,2] and has recently been discussed by Alivisatos.[3] In the formed aggregates, the crystalline lattice planes can be almost perfectly aligned or dislocated at the contact areas between the adjacent particles, where the latter leads to defects in the finally formed product. Pacholski et al. provided further evidence for the oriented-attachment mechanism and showed that a single perfect ZnO nanorod can be conveniently self-assembled from small ZnO quasispherical nanoparticles.[4] Another observed that self-assemblies are analogous to entropy-driven liquid-crystalline phases, as originally proposed by Onsager.[5,6] Therein, side-by-side ordering occurs to maximize the entropy of the self-assembled structure by minimizing the excluded volume per particle in the array. Driving forces including capillary effects,[7] surface tension,[8] chemical bonding,[9] hydrogen bonding,[10] electric[11] and magnetic[12] forces, and hydrophobic interactions[13] have been utilized in various organization schemes.

In progressive structures, a hierarchical nanoarchitecture assembled from nanoscale units provides potential for obtaining higher functionality and performance. Self-assembly has become an important approach for the fabrication of sophisticated architectures. For instance, hierarchical ZnO[14] and MnO_2,[15] featherlike $BaWO_4$,[16] 3D dendritic CuO[17] and Fe_2O_3,[18] and dandelionlike CuO[19] and ZnO[20] nanostructures have been successfully prepared. The fabrication of a hierarchical morphology provides new forms with extremely high surface-to-volume ratios for applications in new catalysts or scaffolding supports and also sheds new insights into the underlying mineralization mechanisms of both natural and synthetic complex nanoarchitectures. However, it is challenging to develop a simple and novel synthetic approach for building hierarchically self-assembled architectures in various systems.

Nanometer-scale aluminum oxide hydroxide (γ-AlOOH) boehmite fibers have been used in the preparation of membranes, catalysts, and coatings on different substrates. Most importantly, alumina and alumina-based composites converted from the fibers have found applications in the field of advanced ceramics.[21−23] The catalytic properties of boehmite or aluminum oxide largely depend on the crystalline structure and texture. The amorphous and semicrystalline nature of aluminum oxides greatly limits their hydrothermal stability and degrades their catalytic properties. Also, textural parameters, such as specific surface area and pore size and shape, determine some technological properties of the catalyst, such as bed volume, accessibility of reactants, and product retention.[24−26] To date, various morphologies of boehmite, such as nanofibers,[27−29] nanotubes,[30,31] and thin plates,[32,33] have been successfully prepared. The hydrothermal synthesis of fiberlike boehmite using basic aluminum chloride as a precursor was originally studied by Bugosh.[27] The procedure has been further developed by many research groups.[34,35] However, to the best of our knowledge, the synthesis of boehmite with hierarchical nanoarchitectures has not yet been reported. Herein, we report a spontaneous and large-scale method to synthesize hierarchical 3D single-crystal boehmite nanoarchitectures with high surface areas.

Experimental Section

AlOOH with 3D nanoarchitectures was prepared by a hydrothermal route using a mixed ethanol−water solution. In a typical experiment, 0.2 g of anhydrate $AlCl_3$ was dissolved in 10 mL of ethanol under vigorous stirring, and then 20 mL of distilled water was added dropwise. The resulting clear and colorless solution was transferred into a Teflon-lined stainless autoclave to fill 85% of the total volume. The autoclave was sealed and maintained at 200 °C for 72 h. The pressure of the sealed autoclave at this temperature was roughly estimated to

* To whom correspondence should be addressed. Fax: + 86-27-67861185. Tel.: +86-27-67861185. E-mail: cctang@phy.ccnu.edu.cn.

10.1021/jp062105f CCC: $33.50
Published on Web 07/04/2006

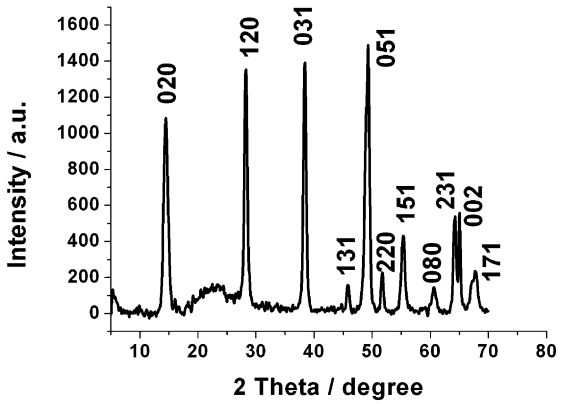

Figure 1. XRD pattern of the product obtained after washing.

be about 1.5 MPa. The autoclave was then allowed to cool naturally to room temperature, and a white precipitated powder was obtained. The powder was filtered and washed several times with absolute ethanol and distilled water and then dried in a vacuum at 60 °C for 12 h. θ-Al_2O_3 flowerlike nanoarchitectures were obtained by annealing the AlOOH nanoarchitectures in air atmosphere at 1000 °C for 5 h.

The crystal structure and phase purity of the product were examined by X-ray diffraction (XRD, D/max-rB, Cu Kα radiation). An overview of the sample morphology was checked with a scanning electron microscope (SEM, JSM-6700F, JEOL), equipped with a system for energy-dispersive X-ray (EDX) analysis. Sample powder was ultrasonically dispersed in acetone and dropped onto a carbon-coated copper grid for transmission electron microscopy (TEM, JEM-2010F, JEOL) analysis. Fourier transform infrared (FTIR) spectroscopy (Nicolet 170-SX) was utilized to characterize the products at vacuum. The products were degassed for more than 2 h to eliminate the absorbed moisture before measurements. Nitrogen adsorption and desorption isotherms at 77 K were measured using a Micrometrics ASAP 2020 V3.00 H system after the sample had been degassed in a vacuum at 120 °C for 400 min.

Results and Discussion

Flowerlike AlOOH nanoarchitectures were synthesized by the hydrothermal reaction of anhydrate $AlCl_3$ in a mixed ethanol−water solution at the appropriate temperature of 200 °C. Considering that anhydrate $AlCl_3$ hydrolyzes strongly in water, absolute ethanol was added first to form an $AlCl_2(OC_3H_5)\cdot(AlCl_3)_2\cdot 10C_2H_5OH$ complex according to the following reaction

$$3AlCl_3 + 11C_2H_5OH \rightarrow AlCl_2(OC_3H_5)\cdot(AlCl_3)_2\cdot 10C_2H_5OH + HCl \quad (1)$$

Therefore, after the water was added, the rate of the hydrolysis reaction between $AlCl_3$ and water could decrease. The low rate was helpful for the formation of nanorods under hydrothermal conditions. The sequence of adding ethanol and water was important for the formation of nanostructures. A typical XRD pattern of the product directly obtained after the washing procedure is shown in Figure 1. All detectable peaks in this pattern can be assigned by their peak positions to orthorhombic γ-AlOOH (JCPDS card no. 21-1307). No evidence could be found for the existence of other impurities in the product after washing.

The morphology of the as-synthesized boehmite nanoarchitectures was examined by SEM. Figure 2 shows SEM micrographs of the obtained product. The low-magnification image

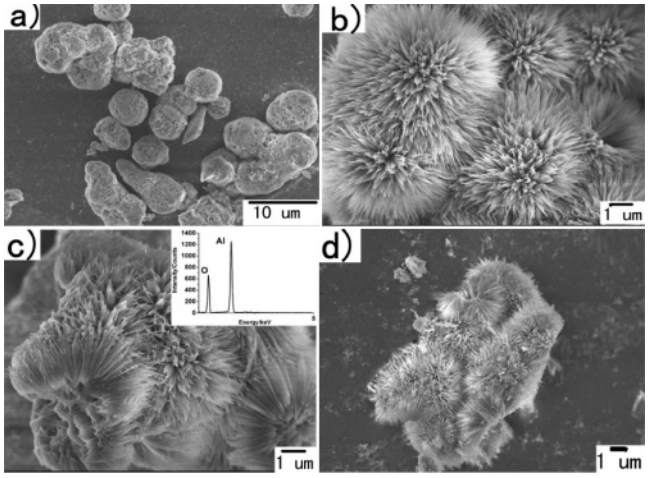

Figure 2. Typical SEM images of the γ-AlOOH nanoarchitectures: (a) low-magnification image; (b) top and (c) lateral views of the flowerlike crystals, (c, inset) EDX spectrum of the product. (d) SEM image of the γ-AlOOH crystals after being annealed at 1000 °C for 5 h.

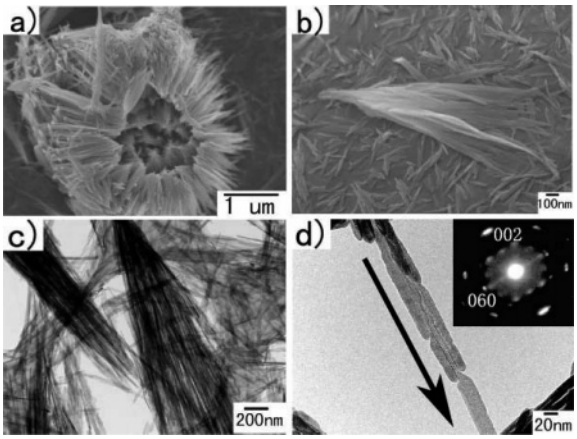

Figure 3. Representative (a,b) SEM and (c,d) TEM images of the γ-AlOOH nanostructures: (a) bottom view, (b) single bundle; c) low-magnification view of bundles, (d) a single nanostrip, (d, inset) SAED pattern of a nanostrip.

(Figure 2a) shows that the AlOOH crystallites self-organize into flowerlike assemblies. Although several semimicrospheres appear to be separate, most particles are attached together to form a larger microsphere aggregate. The structural integrity of the semimicrospheres is not good, and they tend to aggregate with each other. To further examine the surface morphology of the flowerlike architectures, a high-magnification SEM image of several semimicrospheres in the top view of the product was recorded, as shown in Figure 2b. The semimicrospheres are actually composed of many radial nanoscal strips with sharp tips. The cross-sectional view in Figure 2c further confirms the semimicrosphere morphology. EDX measurements were conducted to determine the elemental constituents of the hierarchical structures (inset, Figure 2c). Quantitative results show that the value of the O/Al atomic ratio is approximately 1.9, which is close to the ideal value of 2, considering the instrumental error.

The detailed structure of the nanoarchitectures is shown in Figure 3. A three-tiered organization of the crystallites is observed. Our SEM results in Figure 3a,b indicate that the flowerlike nanoarchitectures are, in fact, composed of broom-shaped bundles that contain even smaller one-dimensional nanostrips with an average length of about 2 μm and a diameter of about 50 nm in the middle section. TEM observation allowed

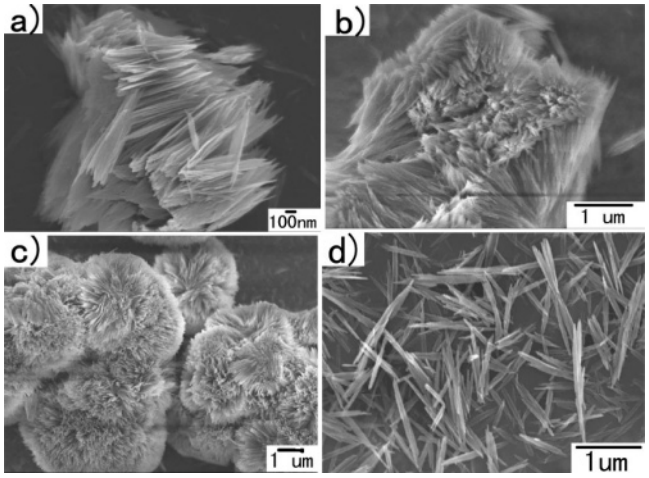

Figure 4. Time-dependent evolution of the flowerlike crystal morphology at different growth stages: (a) 2, (b) 36, and (c) 48 h. (d) SEM image showing that irregular nanorods were formed in the absence of anhydrous ethanol when other conditions were kept constant.

us to confirm the three-tiered structure. A low-magnification TEM image of two bundles (the third tier) is shown in Figure 3c; these might be detached parts from the flowerlike nanoarchitectures or particles that did not aggregate into flower structures. Figure 3d shows the general conformation of a single nanostrip (the second tier), from which we can see that the nanostrip is composed of many nanorods (the first tier). The nanorods are each aligned along the main crystallographic axis of AlOOH, as shown by the arrow. The selected-area electron diffraction (SAED) pattern (inset in Figure 3d) recorded from a single nanostrip indicates that the overall assembly is essentially single-crystalline with a preferential growth direction along the axis perpendicular to the (002) planes. In addition, the SAED pattern is characterized by symmetrical stripes rather than polycrystalline circles or single-crystal spots, implying the presence of some ordered arrangement of crystallites in the nanostrip, which is in good agreement with the TEM observations.

To investigate the formation process of the flowerlike nanoarchitectures, samples subjected to different reaction durations were studied by SEM. Our time-dependent experiments indeed agree with the self-assembly mechanism described above. Three obvious evolutionary stages can be clearly observed and are shown in Figure 4. Under the present synthetic conditions, bundles of nanostrips formed after treatment for 24 h (Figure 4a). The ends of the bundles gradually organized into larger flowerlike bundles when the reaction time was extended to 36 h (Figure 4b). Figure 4c shows that flowerlike 3D nanoarchitectures finally formed after 48 h treatment. A plumper and puffier morphology was observed in the final stage, identical to that shown in Figure 2. From the observed morphologies of the products at different evolutionary stages, a possible formation process is proposed. (1) First, the addition of water to the $AlCl_3$ ethanol solution led to the formation of amorphous $Al(OH)_3$ colloids. The amount of $Al(OH)_3$ colloids formed at this stage was small, and no precipitation was visible. When the reaction was carried out at 200 °C, AlOOH was obtained from the previously formed $Al(OH)_3$ colloids. According to Pierre and Uhlmann,[36] oxygen ions are arranged in a distorted octahedral configuration around aluminum in the boehmite lattice and are organized in parallel layers linked by hydrogen bonds. Because of the presence of weak hydrogen bonds and the interaction between the solvent molecules and the surface OH^- groups via hydrogen bonds, layered AlOOH tends to curl

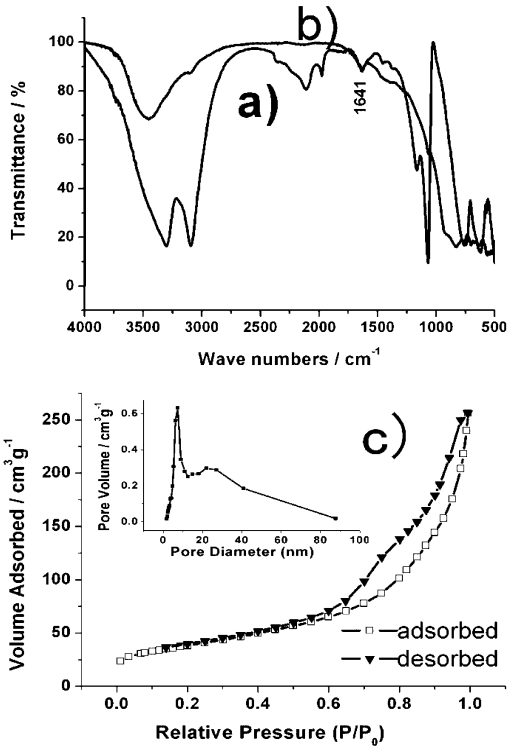

Figure 5. FTIR reflection spectra of (a) γ-AlOOH and (b) θ-Al_2O_3 after being annealed at 1000 °C for 5 h. (c) N_2 absorption and desorption isotherms and (insets) pore size distributions for the γ-AlOOH nanoarchitectures.

at elevated temperature and pressure, leading to the formation of one-dimensional AlOOH nanorods via a rolling mechanism. This is a general process for the formation of nanorods through the folding of lamellae.[37,38] (2) As the reaction proceeded, the formed nanorods began to arrange along the main crystallographic axis of the [001] direction to form nanostrips, possibly via an oriented-attachment process (inset in Figure 3d).[1−3] The formation of nanostrips is possibly related to the hydrogen bonds on the surface of the nanorods. To confirm this possibility, FTIR measurements were conducted on a sample containing flowerlike AlOOH nanoarchitectures, as shown in Figure 5a. The absorption edge of the hydroxyl bands on the surface was found at 1641 cm^{-1}.[31] More convincing evidence could be found from the FTIR measurements on the θ-Al_2O_3 sample, which were obtained after annealing the AlOOH nanoarchitectures at 1000 °C for 5 h. The hydroxyl bands at 1641 cm^{-1} can be still observed (Figure 5b), and the flowerlike morphology is still retained (Figure 2d). This indicates a high capacity of the alumina phases to retain the hydroxyls. In addition, the polarity and steric bulkiness around the hydroxyl groups of the ethanol possibly affect the product morphology.[39] However, not all nanorods could self-assemble into nanostrips, as we observed some fragmentary nanorods around the bundles of nanostrips in Figure 3c. (3) Because of the presence of hydroxyl groups on the surface of the nanorods and in the ethanol solvent, the lateral arrangement of these nanostrip units would naturally lead to the formation of bundles shown in Figure 4a. After a longer reaction time, bundles surrounded by nanostrips gradually gathered together into larger broomlike ones (Figure 4b). Finally, the flowerlike 3D nanoarchitectures were formed.

From the formation process discussed above, we believe that the absolute ethanol plays a key role in the formation of the as-synthesized product. To examine the function of ethanol, a comparative experiment in the absence of absolute ethanol was

also carried out. The hydrothermal reaction of $AlCl_3$ in water alone resulted in AlOOH nanorods with an irregular morphology. A typical morphology is shown in Figure 4d. The added ethanol reacts with $AlCl_3$ to form a complex of $AlCl_2(OC_3H_5)\cdot(AlCl_3)_2\cdot 10C_2H_5OH$, causing $AlCl_3$ to hydrolyze slowly to form $Al(OH)_3$. As is known, it is difficult to produce well-controlled hierarchical morphologies such as architectures by directly mixing two incompatible solutions of metal salts because of a rapid decrease in the degree of supersaturation and the consequent depletion of reaction components in a short period of time.[17] Therefore, the coordinated $AlCl_2(OC_3H_5)\cdot(AlCl_3)_2\cdot 10C_2H_5OH$ could separate the processes of nucleation and growth, which is helpful for the formation of nanorods. In addition, hydrogen bonds between ethanol and the hydroxyl groups on the surface of nanorods are responsible for the formation of the self-assemble of bundles.

Brunauer−Emmett−Teller (BET) gas-sorption measurements were conducted to examine the porous nature of the boehmite nanoarchitectures. The recorded absorption and desorption isotherms for the AlOOH boehmite show a significant hysteresis at relative pressures P/P_0 above 0.45 (Figure 5c). The isotherms are identified as type IV, which is characteristic of mesoporous materials. Barrett−Joyner−Halenda calculations for the pore-size distribution, derived from desorption data, reveal a narrow distribution for the boehmite nanoarchitectures centered at 6−7 nm (Figure 5c, inset). The BET specific surface area of the sample calculated from N_2 isotherms at 77 K was found to be as high as about 137.2 $m^2\ g^{-1}$, which is the same as that of single-crystalline boehmite nanotubes.[30] However, the specific area decreases considerably with increasing boehmite crystallinity. The highest surface area reported so far for a crystallized sample is 91 $m^2\ g^{-1}$,[22] whereas the AlOOH nanoarchitectures obtained here have an extremely high BET area and display excellent porous properties.

Conclusions

In summary, the progressive production of flowerlike AlOOH (boehmite) 3D nanoarchitectures formed of nanostrips has been demonstrated in the absence of any templates or matrixes. The formation of such structures requires a suitable $AlCl_3$ complex precursor that slowly dissociates to yield $Al(OH)_3$ colloids under hydrothermal conditions. Hydrogen bonds on the surface of the nanorods or nanostrips possibly play a key role. Although the formation mechanism of 3D nanoarchitectures is not yet fully understood, this work shows a perspective that elaborately self-organized architectures can be controllably synthesized. Taking into account the characteristics of single crystallinity and high BET surface area, the AlOOH nanoarchitectures developed in the present work are promising candidates for technical applications as catalyst, sorbent, ceramic, and optical nanodevices.

Acknowledgment. This work was supported by the Fok Ying Tong Education Foundation (Grant 91050) and the NNSF of China (Grant 50202007).

References and Notes

(1) Penn, R. L.; Banfield, J. F. *Science* **1998**, *281*, 969.
(2) Banfield, J. F.; Welch, S. A.; Zhang, H.; Ebert, T. T.; Penn, R. L. *Science* **2000**, *289*, 751.
(3) Alivisatos, A. P. *Science* **2000**, *289*, 736.
(4) Pacholski, C.; Kornowski, A.; Weller, H. *Angew. Chem., Int. Ed.* **2002**, *41*, 1188.
(5) Onsager, L. *Ann. N.Y. Acad. Sci.* **1949**, *51*, 627.
(6) Nikoobakht, B.; Wang, Z. L.; ElSayed, M. A. *J. Phys. Chem. B* **2000**, *104*, 8635.
(7) Bowden, N.; Terfort, A.; Carbeck, J.; Whitesides, G. M. *Science* **1997**, *276*, 233.
(8) Velikov, K. P.; Christova, C. G.; Dullens, R. P. A.; Blaaderen, A. *Science* **2002**, *296*, 106.
(9) Mayer, C. R.; Neveu, S.; Cabuil, V. *Adv. Mater.* **2002**, *14*, 595.
(10) Whitesides, G. M.; Grzybowski, B. *Science* **2002**, *295*, 2418.
(11) Gracias, D. H.; Tien, J.; Breen, T. L.; Hsu, C.; Whitesides, G. M. *Science* **2000**, *289*, 1170.
(12) Love, J. C.; Urbach, A. R.; Prentiss, M. G.; Whitesides, G. M. *J. Am. Chem. Soc.* **2003**, *125*, 12696.
(13) Park, S.; Lim, J. H.; Chung, S. W.; Mirkin, C. A. *Science* **2004**, *303*, 348.
(14) Lao, J. Y.; Wen, G. J.; Ren, Z. F. *Nano Lett.* **2002**, *2*, 1287.
(15) Li, Z. Q.; Ding, Y.; Xiong, Y. J.; Yang, Q.; Xie, Y. *Chem. Commun.* **2005**, *7*, 918.
(16) Shi, H. T.; Qi, L. M.; Ma, J. M.; Cheng, H. M. *J. Am. Chem. Soc.* **2003**, *125*, 3450.
(17) Zhang, Z. P.; Shao, X. Q.; Yu, H. D.; Wang, Y. B.; Han, M. Y. *Chem. Mater.* **2005**, *17*, 332.
(18) Cao, M. H.; Liu, T. F.; Gao, S.; Sun, G. B.; Wu, X. L.; Hu, C. W.; Wang, Z. L. *Angew. Chem., Int. Ed.* **2005**, *44*, 4197.
(19) Liu, B.; Zeng, H. C. *J. Am. Chem. Soc.* **2004**, *126*, 8124.
(20) Liu, B.; Zeng, H. C. *J. Am. C*hem. Soc. **2004**, *126*, 16744.
(21) Yoldas, B. E. *J. Mater. Sci.* **1975**, *10*, 1856.
(22) Music, S.; Dragcevic, O.; Popovic, S. *Mater. Lett.* **1999**, *40*, 269.
(23) Raybaud, P.; Digne, M.; Iftimie, R.; Wellens, W.; Euzen, P.; Toulhoat, H. *J. Catal.* **2001**, *201*, 236.
(24) Mishra, D.; Anand, S.; Panda, R. K.; Das, R. P. *Mater. Lett.* **2000**, *42*, 38.
(25) Tsuchida, T. *J. Eur. Ceram. Soc.* **2000**, *20*, 1759.
(26) Vaudry, F.; Khodabandeh, S.; Davis, M. E. *Chem. Mater.* **1996**, *8*, 1451.
(27) Bugosh, J. *J. Chem. Phys.* **1961**, *65*, 1789.
(28) Buining, P. A.; Pathmamanoharan, C.; Jansen, J. B. H.; Lekkerkerker, H. N. W. *J. Am. Ceram. Soc.* **1991**, *74*, 1303.
(29) Kuiry, S. C.; Megen, E.; Patil, S. D.; Deshpande, S. A.; Seal, S. *J. Phys, Chem. B* **2005**, *109*, 3868.
(30) Kuang, D. B.; Fang, Y. P.; Liu, H. Q.; Frommen, C.; Fenske, D. *J. Mater. Chem.* **2003**, *13*, 660.
(31) Hou, H. W.; Xie, Y.; Yang, Q.; Guo, Q. X.; Tan, C. R. *Nanotechnology* **2005**, *16*, 741.
(32) Lippens, B. C.; de Boer, J. H. *Acta Crystallogr.* **1964**, *17*, 1312.
(33) Van der Kooij, F. M.; Lekkerkerker, H. N. W. *J. Phys. Chem. B* **1998**, *102*, 7829.
(34) Buining, P. A.; Philipse, A. P.; Lekkerkerker, H. N. W. *Langmuir* **1994**, *10*, 2106.
(35) Gabriell, J. C. P.; Davidson, P. *Top. Curr. Chem.* **2003**, *226*, 119.
(36) Pierre, A. C.; Uhlmann, D. R. *J. Non-Cryst. Solids* **1986**, *82*, 271.
(37) Li, Y. D.; Li, X. L.; Deng, Z. X. *Angew. Chem., Int. Ed.* **2002**, *41*, 333.
(38) Wang, X.; Li, Y. D. *Chem. Eur. J.* **2003**, *9*, 300.
(39) Inoue, M.; Kimura, M.; Inui, T. *Chem. Mater.* **2000**, *12*, 55.